Magnetic Resonance Imaging 113 (2024) 110214

Contents lists available at ScienceDirect

Magnetic Resonance Imaging

journal homepage: www.elsevier.com/locate/mri

DCE-MRI Radiomic analysis in triple negative ductal invasive breast cancer. Comparison between BRCA and not BRCA mutated patients: Preliminary results

Annarita Pecchi [a], Chiara Bozzola [a], Cecilia Beretta [a], Giulia Besutti [a,b,*], Angela Toss [c], Laura Cortesi [c], Erica Balboni [d], Luca Nocetti [d], Guido Ligabue [a], Pietro Torricelli [a]

[a] Division of Radiology, Department of Medical and Surgical Sciences of Children and Adults, University of Modena and Reggio Emilia, 41224 Modena, Italy
[b] Radiology Unit, Department of Diagnostic Imaging and Laboratory Medicine, AUSL-IRCCS di Reggio Emilia, Via Risorgimento 80, 42123 Reggio Emilia, Italy
[c] Division of Oncology, Department of Medical and Surgical Sciences of Children and Adults, University of Modena and Reggio Emilia, 41224 Modena, Italy
[d] Medical Physics Unit, University Hospital of Modena, 41124 Modena, Italy

ARTICLE INFO

Keywords:
Radiogenomics
Magnetic resonance imaging
Breast cancer
BRCA1 gene

ABSTRACT

Objective: The research aimed to determine whether and which radiomic features from breast dynamic contrast enhanced (DCE) MRI could predict the presence of BRCA1 mutation in patients with triple-negative breast cancer (TNBC).
Material and methods: This retrospective study included consecutive patients histologically diagnosed with TNBC who underwent breast DCE-MRI in 2010–2021. Baseline DCE-MRIs were retrospectively reviewed; percentage maps of wash-in and wash-out were computed and breast lesions were manually segmented, drawing a 5 mm-Region of Interest (ROI) inside the tumor and another 5 mm-ROI inside the contralateral healthy gland. Features for each map and each ROI were extracted with Pyradiomics-3D Slicer and considered first separately (tumor and contralateral gland) and then together. In each analysis the more important features for BRCA1 status classification were selected with Maximum Relevance Minimum Redundancy algorithm and used to fit four classifiers.
Results: The population included 67 patients and 86 lesions (21 in BRCA1-mutated, 65 in non BRCA-carriers). The best classifiers for BRCA mutation were Support Vector Classifier and Logistic Regression in models fitted with both gland and tumor features, reaching an Area Under ROC Curve (AUC) of 0.80 (SD 0.21) and of 0.79 (SD 0.20), respectively. Three features were higher in BRCA1-mutated compared to non BRCA-mutated: Total Energy and Correlation from gray level cooccurrence matrix, both measured in contralateral gland in wash-out maps, and Root Mean Squared, selected from the wash-out map of the tumor.
Conclusions: This study showed the feasibility of a radiomic study with breast DCE-MRI and the potential of radiomics in predicting BRCA1 mutational status.

1. Introduction

Triple-negative breast cancer (TNBC), accounting for 15–25% of all breast cancers, is a specific subtype that does not express estrogen receptor (ER), progesterone receptor (PR) or human epidermal growth factor receptor 2 (HER-2). It has clinical features that include high invasiveness, high metastatic potential, proneness to relapse and poor prognosis [1,2].

BRCA1 and BRCA2 are tumor suppressor genes, the mutant phenotypes of which predisposes patients to breast and ovarian cancers [3,4]. In particular, breast cancer in BRCA1 carriers tends to present as TNBC with atypical morphologic features and more aggressive behaviour [5,6] whereas BRCA2-related tumors are much more similar to sporadic cancer [7–9]. Several studies have been conducted to examine the relationships between BRCA1/2 mutations and breast cancer MRI features, suggesting that MRI features can differ according to BRCA mutation type and reflect intrinsic hereditary characteristics [9,10]. In addition, other studies are recently investigating the role of radiomics in breast imaging to provide further information about tumor characterization.

* Corresponding author at: Department of Medical and Surgical Sciences of Children and Adults, University of Modena and Reggio Emilia, 41224 Modena, Italy.
E-mail addresses: giulia.besutti@ausl.re.it, giulia.besutti@unimore.it (G. Besutti).

https://doi.org/10.1016/j.mri.2024.110214
Received 13 May 2024; Received in revised form 17 July 2024; Accepted 20 July 2024
Available online 22 July 2024

Radiomics is the process of extracting quantitative properties, named features, from an entire image or from a specific region of interest (ROI) which collectively provide a comprehensive tumor characterization, called "the radiomic signature of the tumor" [11,12]. The feature extraction process is typically realized using pattern recognition algorithms, calculating a set of variables representing a quantitative description of a geometrical or physical property of the image portion under consideration. Radiomics is based on the hypothesis that the extracted features reflect mechanisms occurring at genetic and molecular levels.

Radiogenomics, relating radiomic features to genomic profile, is being increasingly used for tumors characterization and is rapidly growing in the field of breast imaging [13,14]. By adding radiomics to the standard radiological workflow, it would be possible to improve diagnostic accuracy of standard radiological techniques such as mammography, tomosynthesis and MRI [15].

Studies have investigated the usefulness and reliability of radiomics in both discriminative tasks (malignant lesion recognition [16], classification of subtype and stage, histological differentiation [17,18]) and predictive tasks (response to therapy, risk of recurrence [19], preoperative prediction of axillary lymph node metastasis [20]).

The potential of MR radiomics alone or combined with clinical features in the non-invasive prediction of BRCA mutational status have been reported in a few studies only, which did not focus on TNBC.

The aim of the study was to analyze whether there are differences in the clinical and radiological characteristics of triple-negative tumors arising in women with or without genetic mutation; secondly to determine whether and which radiomic features extracted from DCE-MRI predict the presence of BRCA1 mutations in patients with TNBC.

2. Material and methods

2.1. Study design

We used the CLEAR checklist (CheckList for Evaluation of Radiomics research) endorsed by ESR and EuSoMII to design and report this manuscript [21].

The research was approved by the Area Vasta Emilia Nord Ethical Committee and informed consent was obtained from all subjects.

This retrospective study included consecutive patients histologically diagnosed with TNBC who underwent breast DCE-MRI between February 2010 and August 2021 on a single 1.5 T MR scanner at a single institution (Azienda Ospedaliero-Universitaria Policlinico di Modena). The criteria for patient inclusion were the histological diagnosis of triple negative ductal invasive breast cancer, the genetic testing result and the availability of DCE-MRI exam acquired on the axial plane with a fat signal suppression at the time of diagnosis.

On the other hand, we excluded patients with unavailability of clinical and pathological data, MRI exams with artifacts and with non-standardized image acquisition protocol, in particular without fat suppression and/or acquired in the coronal plane.

2.2. Clinical and radiological data collection

Data were collected with the collaboration of Centro Oncologico Modenese (COM) and analyzed with the collaboration of the Medical Physics Unit at Azienda Ospedaliero-Universitaria Policlinico di Modena.

Breast MRI exams were performed on 1.5 Tesla magnet (Philps Achieva software version 2.6 and 3.2) using 7 channel dedicated surface breast coil. All the dynamic sequences were acquired on the axial plane with a fat-suppressed 3D-T1-weighted sequence, namely T1 High Resolution Isotropic Volume Excitation (THRIVE) (TR 7 s, TE 3 ms, FA 12°, pixel dimensions 0.7 × 0.7 × 1 mm^3, using Spectral Attenuated Inversion Recovery - SPAIR - for fat suppression) or Water Selective Excitation (WATS) (TR 15 s, TE 5 ms, FA 20°, pixel dimensions 0.7 × 0.7 × 1 mm^3), with one phase before and 5 phases after intravenous administration of gadolinium-based contrast agent (Dotarem 0,2 ml/kg) with an injection rate of 2 ml/s to cover a time span of 10 min.

Collected non-radiomics data were breast density in accordance with the recommendations of the proposed American College of Radiology Breast Imaging Reporting and Data System (BI-RADS); Background Parenchymal Enhancement (BPE), classified using the BI-RADS four-point scale as minimal, mild, moderate, or marked; enhancement curve, referring to the contrast enhancement kinetics of a lesion, classified in type 1 (progressive or persistent enhancement pattern, usually considered benign), type 2 (wash in – plateau pattern, considered undetermined) and type 3 (wash in – wash out pattern, considered strongly suggestive of malignancy); the shape of the lesion (mass-like/non mass-like); the extent of disease, classified in single lesion, multifocal (the presence of two or more foci of cancer within the same breast quadrant) or multicentric (the presence of two or more foci of cancer in different quadrants of the same breast) and tumor volume (cm^3).

2.3. Radiomic analysis

Breast MRI studies were retrospectively reviewed to collect radiomic data of the tumor and the contralateral gland, which were manually segmented by two radiologists in consensus. Radiomic data were compared between tumors and contralateral gland of BRCA-mutated and non-BRCA mutated women and different radiomic classifier were tested to predict mutational status.

2.3.1. Segmentation

The second phase acquired after contrast administration, was used for tumor segmentation, performed manually through a contouring tool in Advantage Workstation 4.7 (GE Healthcare). This first segmentation was volumetric and conducted including the whole tumor (or the tumors, where more than one lesion was present).

Then, two round-shaped 5 mm-diameter Regions of Interest (ROIs) were drawn respectively inside the volume of the isolated tumor and inside the normal glandular tissue of the contralateral breast, in the most homogeneous region, avoiding necrotic tissue, blood vessels and prothesis. When multiple tumors were present in a single patient, all tumors of at least 5 mm diameter were segmented.

2.3.2. Pre-processing

The preprocessing consisted of calculating two percentage maps from the contrastographic images, one for the wash-in and one for the wash-out of the contrast medium. The wash-in analysis was computed from the peak phase after contrast administration, while the last phase was used to obtain the wash-out analysis, for both the ROI in the tumor and the ROI in the contralateral gland.

The wash-in map was calculated as the difference between the peak post-contrastographic and the pre-contrastographic phase divided by the pre-contrastographic phase.

Similarly, the wash-out map was the difference between the last post-contrastographic and the peak post-contrastographic phase over the peak post-contrastographic phase, multiplying by 10^5 to avoid information loss due to the only availability of integer numbers for image computation in the software. The peak phase was assumed to correspond to the phase with the maximum average intensity inside the tumor and gland ROIs:

$$wash_{in} = \frac{peak - 1^{st}}{1^{st}} * 10^5$$

$$wash_{out} = \frac{last - peak}{peak} * 10^5$$

Using this method, we did not consider the wash-in and wash-out of each voxel, but voxel intensity at wash-in and wash-out of the entire ROIs.

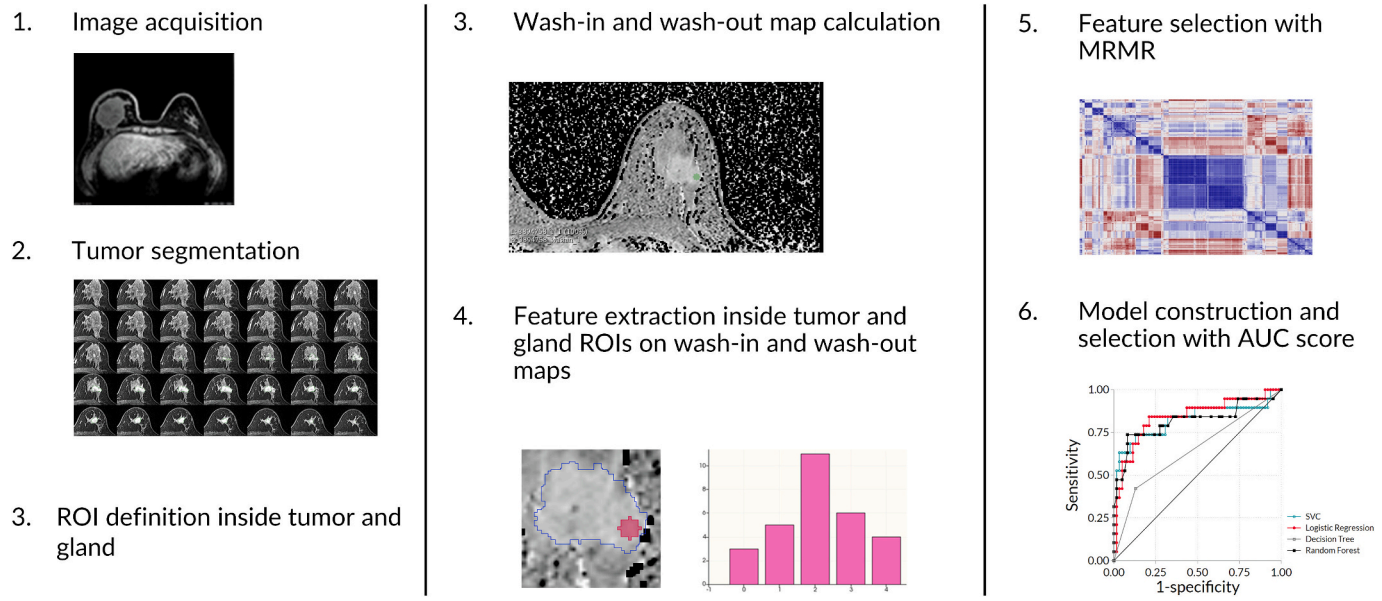

Fig. 1. Flowchart of the study pipeline.

For image preprocessing, we executed a custom Python routine using the 3D Slicer API [22].

2.3.3. Features extraction

Radiomic features were extracted from the 5 mm ROIs (described in the Segmentation section) and not from the volumetric segmentation of the whole tumor, in order to obtain more homogenous data. Features for each map and each ROI were extracted with the Pyradiomics extension of 3D Slicer, using a bin width of 100 and a symmetrical Gray Level co-occurrence matrix. The other extraction parameters were left as default.

We extracted all the available features except for shape features since the considered ROIs had the same shape.

2.3.4. Features selection and data preparation

The processing of the extracted features and the statistical analyses were performed through a Stata 17 code with Python 3.8 integration, using the Python libraries SK-learn v. 1.0.2, and Numpy v. 1.24.4. The extracted features were standardized by subtracting the mean value and dividing by the standard deviation. We first considered separately the features from the tumor and the contralateral gland, then we performed another analysis with all the features together. For completeness we considered also other 4 possibilities including separately wash-in and wash-out features from gland and wash-in and wash-out features from tumor.

For dimensionality reduction, the most important and discriminative features for BRCA1 status classification were selected with Maximum Relevance Minimum Redundancy algorithm. To decide the number of selected features we visually inspected the correlation heat-plot of all the features, showing the Spearman correlation matrix in colour scale, with rows and columns sorted by similarity via hierarchical clustering.

2.3.5. Modelling

The selected features in each analysis were used to train 4 classifiers, one linear, Logistic Regression, and the other ones nonlinear, which were Support Vector Classifier (SVC), Random Forest and Decision Tree. The setting parameters were left as default, i.e. SVC with 1 as regularization parameter; Random Forest with 100 estimators and no maximum depth, as well as for Decision Tree. A covariate variable was introduced to take into account the different acquisition protocol.

Table 1
Descriptive statistics of the study population.

	BRCA1 (n = 18)	NON-BRCA MUTATED (n = 49)	OVERALL (n = 67)
Age			
	42.44 ± 10.56	48.23 ± 9	46.68 ± 9.70
Breast density[a]			
A	1 (5.9%)	5 (10.2%)	6 (9.1%)
B	8 (47.1%)	16 (32.7%)	24 (36.4%)
C	4 (23.5%)	21 (42.9%)	25 (37.9%)
D	4 (23.5%)	7 (14.3%)	11 (16.7%)
BPE[a]			
Minimal	1 (5.9%)	2 (4.1%)	3 (4.5%)
Mild	6 (35.3%)	24 (49%)	30 (45.5%)
Moderate	8 (47.1%)	12 (24.5%)	20 (30.3%)
Marked	2 (11.8%)	11 (22.4%)	13 (19.7%)
Shape of the lesion			
Mass	18 (100%)	39 (79.6%)	57 (85.1%)
Non Mass		8 (16.3%)	8 (11.9%)
Mass + Non Mass		2 (4.1%)	2 (3%)
Enhancement curve			
1–2	1 (5.6%)		1 (1.5%)
2	4 (22.2%)	5 (10.2%)	9 (13.4%)
2–3	2 (11.1%)	14 (28.6%)	16 (23.9%)
3	11 (61.1%)	30 (61.2%)	41 (61.2%)
Extent of disease			
Single	11 (61.1%)	21 (42.9%)	32 (47.8%)
Multifocal	2 (11.1%)	12 (24.5%)	14 (20.9%)
Multicentric	5 (27.8%)	16 (32.7%)	21 (31.3%)
Volume of the lesion			
	9,62 ± 15,91	13,3 ± 17,38	11,9 ± 16,79

BPE, background parenchymal enhancement.

[a] Breast density and BPE were not evaluated in one BRCA-mutated patient who already underwent mastectomy and had breast prosthesis implantation at TNBC diagnosis time.

2.3.6. Evaluation

The models were internally tested through stratified 10-fold cross validation by permuting 10 times the training (90% of the entire sample) and the testing dataset (10%). Furthermore, the stratified cross validation allowed to keep the same percentage of patients with and without the mutation in each permutation, balancing the two groups.

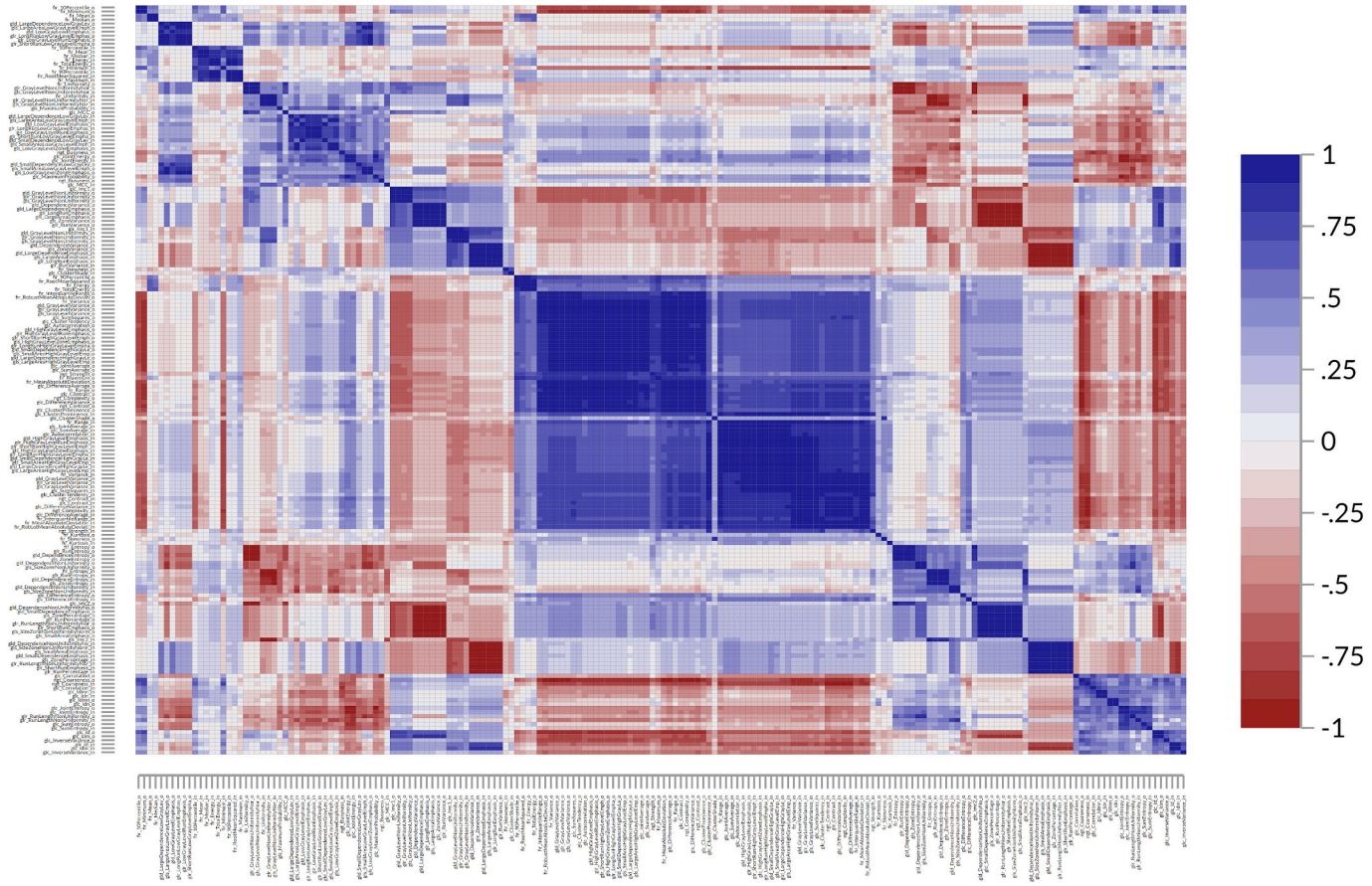

Fig. 2. Correlation heat-map of the features from gland segmentations, showing Spearman's correlation coefficient for each couple of features with a red-blue colormap. The features were grouped based on a similarity clustering algorithm. (For interpretation of the references to colour in this figure legend, the reader is referred to the web version of this article.)

For each model and permutation, we calculated the Area Under ROC Curve (AUC), the accuracy, the sensitivity, and the specificity. The sensitivity and specificity were computed at their optimal value in the ROC curve, maximizing their geometric mean. Then, we considered the mean and the standard deviation (SD) of these scores across the 10 permutations. The discriminant metric to identify the best model was AUC.

To evaluate if the different models were significantly different, we used the McNemar's test [23].

The entire workflow is summarized in Fig. 1.

3. Results

3.1. Baseline demographic and clinical characteristics

Among patients with TNBC histological diagnosis from February 2010 to August 2021, we retrospectively selected 69 patients with an available baseline MRI exam and the results of genetic testing on BRCA. BRCA2 carriers ($n = 2$) were excluded for the limited sample size and different clinical radiological tumor pattern, according to the literature [23].

The final population included 67 patients (mean age 46,68 ± 9,70 years), 18 of which were BRCA1 mutated and 49 were non-BRCA mutated. Some patients had multiple lesions for a total of 86 lesions analyzed (21 in BRCA1 mutated, 65 in non-BRCA mutated).

Characteristics of study population are shown in Table 1.

3.2. Radiomic features analysis

The total number of extracted features was 372, classified in first-order, second-order and features from texture analysis. In particular, we extracted 21 intensity-based first-order statistical features, 23 Gy level cooccurrence matrix (GLCM) features (second-order), 11 Gy level size zone matrix (GLSZM) features, 16 Gy level run length matrix (GLRLM) features, 3 neighborhood gray-tone difference matrix (NGTDM) features, 12 Gy level dependence matrix (GLDM) features.

Correlation heat-maps showed that almost 4 radiomic features from tumor segmentations and 4 from gland segmentations were sufficiently independent to be used in the final model without redundancies (Figs. 2–4). Hence, we set the number of selected features to 8 in the model including both tumor and gland features and 4 for the 2 sub-models. In the models fitted with only wash-out and wash-in features we also considered 4 most relevant features (Supplementary Figs. S1-S4).

According to the AUC parameter, the best classifiers for BRCA mutational status were SVC and Logistic Regression in models fitted with both gland and tumor features (Table 2). The features selected for the comprehensive model were Total Energy (first level), Correlation (GLCM) and Long Run Low Gray Level Emphasis (GLRLM) from gland wash-out map; Kurtosis (first level) and Small Area Low Gray Level Emphasis (GLSZM) from gland wash-in map; Root Mean Squared (first level) and Large Dependence Emphasis (GLDM) from tumor wash-out map; Strength (NGTDM) from tumor wash-in map.

The models computed with gland features only reached similar scores of the ones with both gland and tumor features, while the models fitted with only tumor features were not able to discriminate mutated

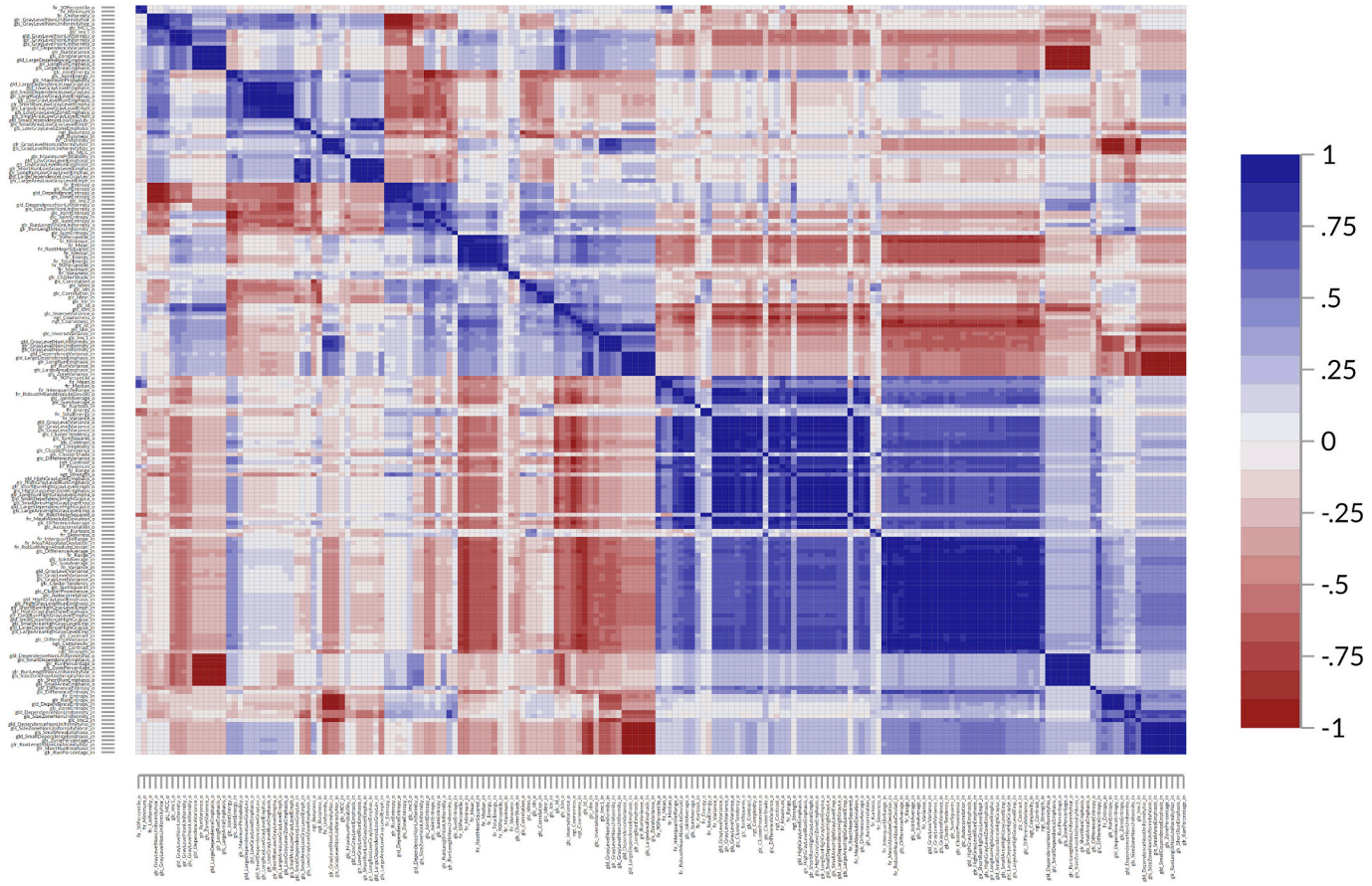

Fig. 3. Correlation heat-map of the features from tumor segmentations, showing Spearman's correlation coefficient for each couple of features with a red-blue colormap. The features were grouped based on a similarity clustering algorithm. (For interpretation of the references to colour in this figure legend, the reader is referred to the web version of this article.)

and non-mutated patients (AUC < 0.6) (Tables 3–4). The features used to fit the models for gland features, with the corresponding statistics referred to the initial unstandardized features, were: Total Energy (first level) from the wash-out map, which was significantly higher in BRCA1-mutated patients ($Median_{BRCA1\text{-}mutated}$ 1.1e+10, $Median_{Non\text{-}mutated}$ 0.54e+10, $_{pWilcoxon} < 0.01$); Small Dependence Low Gray Level Emphasis (GLDM), computed in the wash-in map; Kurtosis (first level) from the wash-in map; Correlation (GLCM), computed in the wash-out map, significantly higher in BRCA1-mutated patients ($Median_{BRCA1\text{-}mutated}$ 0.25, $Median_{non\text{-}mutated}$ 0.12, $p_{Wilcoxon} < 0.01$).

Finally, selected features from tumor segmentation were Root Mean Squared (first level) from the wash-out map, significantly higher in BRCA1-mutated patients ($Median_{BRCA1\text{-}mutated}$ 14e+03, $Median_{non\text{-}mutated}$ 11e+03, $p_{Wilcoxon} < 0.05$); Size Zone Non Uniformity (GLSZM), computed in the wash-out map; IMC2 (GLCM), computed in the wash-in map; and Maximum (first level) from the wash-in map.

The models fitted with only wash-in and wash-out features reached lower scores (AUC < 0.7) than the models fitted with features from both maps (Supplementary Tables S1-S4).

The McNemar's tests showed that there was a significant difference ($p < 0.05$) between the SVC model from tumor features and all the other models, while all the other comparisons resulted in a p value higher than 0.05.

3.3. Association of non-radiomic features variables with the outcome

Among clinical characteristics, a statistically significant difference (p value 0,03) was obtained only for age at diagnosis of breast cancer, with an average age at diagnosis in patients BRCA1 mutated of 42,44 years and in patients non BRCA mutated of 48,2.

No statistically significant differences were observed between the two groups about the other clinical data, like breast density, BPE, enhancement curve and disease extent.

All BRCA-mutated patients had mass-like lesions, while non BRCA-mutated lesions were more heterogeneous (79,6% mass-like, 16,3% non-mass like, 4,1% both).

4. Discussion

In this retrospective study, we reviewed the breast-MRI exams of 67 TNBC patients, BRCA1-mutated (18) and non-BRCA mutated (49), for a total of 21 and 65 lesions respectively analyzed. We considered the numerical disparity between the two groups, during validation of radiomics analysis model, by performing a balanced cross validation.

Firstly, a statistical analysis was initially conducted to describe general characteristics of the two populations and breast lesions at MRI.

As to general characteristics, BRCA1-mutated patients were younger (mean age 42 vs 48 years), but no other statistically significant differences were found [24,25].

With respect to the lesion characteristics, in both groups the tumors were more frequently single and presented as mass-like lesion, with a type 3 enhancement curve [24–26].

The breast composition, the enhancement of the glandular tissue, the morphology and/or enhancement of the lesion, usually considered at MRI examination, did not show significant differences between patients carrying and not carrying BRCA1 mutation. There are no gland and/or tumor characteristics significantly related to the genetic mutation.

Secondly, we investigated the potential role of radiomic analysis in

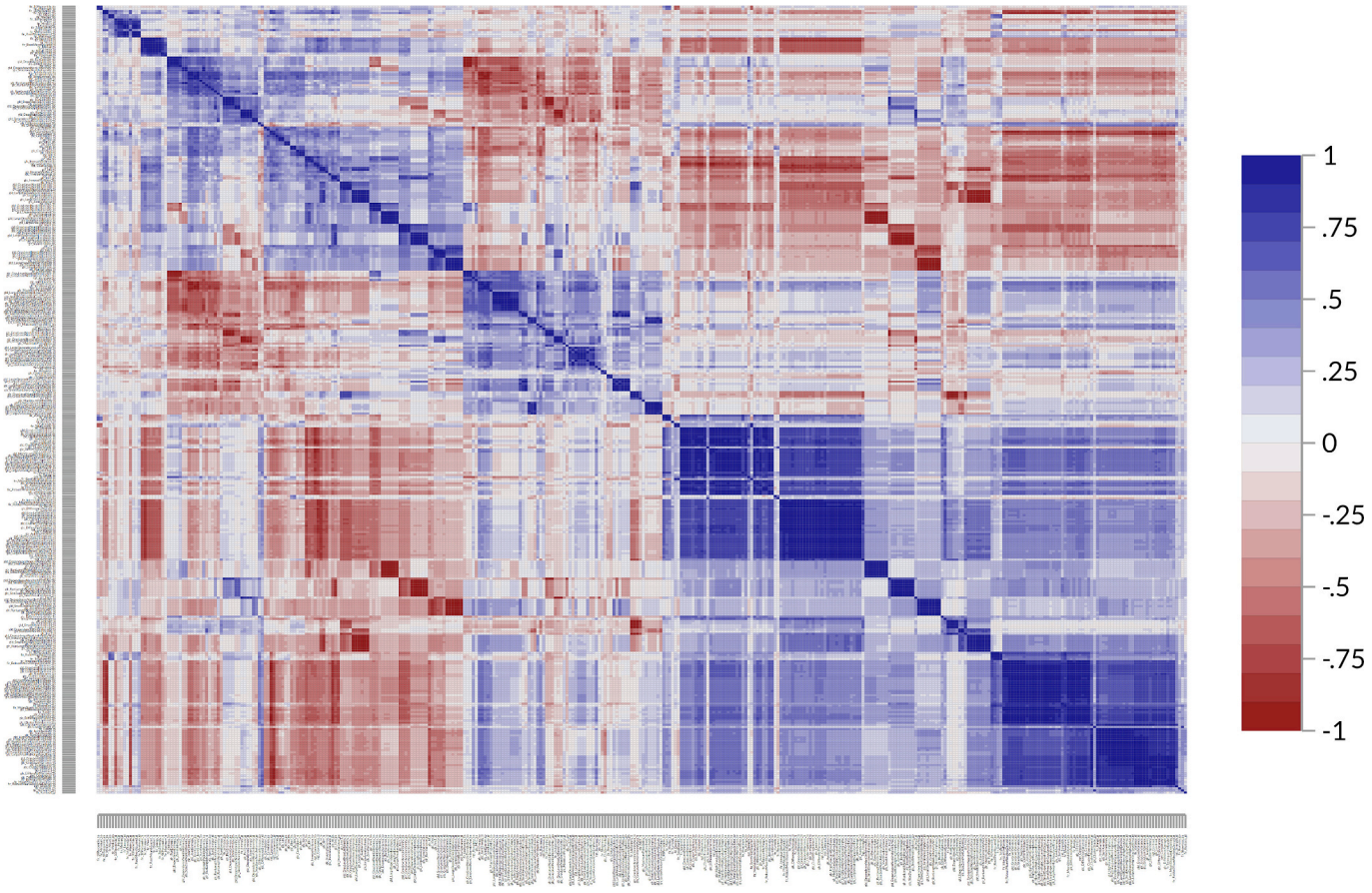

Fig. 4. Correlation heat-map of the features from gland and tumor segmentations, showing Spearman's correlation coefficient for each couple of features with a red-blue colormap. The features were grouped based on a similarity clustering algorithm. (For interpretation of the references to colour in this figure legend, the reader is referred to the web version of this article.)

Table 2
Scores of the considered classifiers fitted with 8 wash-in and wash-out gland and tumor features, selected with MRMR. Mean and standard deviation (SD) values from the 10 cross validation splits of the dataset are reported.

Model	AUC	Accuracy	Sensitivity	Specificity
	Mean (SD)	Mean (SD)	Mean (SD)	Mean (SD)
SVC	0.80 (0.21)	0.79 (0.10)	0.90 (0.20)	0.82 (0.17)
Random Forest	0.74 (0.35)	0.78 (0.12)	0.85 (0.32)	0.80 (0.24)
Decision Tree	0.69 (0.20)	0.70 (0.16)	0.65 (0.45)	0.78 (0.23)
Logistic Regression	0.79 (0.20)	0.79 (0.12)	0.85 (0.23)	0.8 (0.20)

AUC, area under the curve; SD, Standard Deviation; SVC, Support Vector Classifier.

Table 3
Scores of the considered classifiers fitted with 4 wash-in and wash-out tumor features, selected with MRMR. Mean and standard deviation (SD) values from the 10 cross validation splits of the dataset are reported.

Model	AUC	Accuracy	Sensitivity	Specificity
	Mean (SD)	Mean (SD)	Mean (SD)	Mean (SD)
SVC	0.59 (0.24)	0.73 (0.05)	0.60 (0.30)	0.57 (0.21)
Random Forest	0.61 (0.18)	0.65 (0.13)	0.80 (0.24)	0.69 (0.21)
Decision Tree	0.48 (0.17)	0.59 (0.16)	0.20 (0.33)	0.92 (0.18)
Logistic Regression	0.60 (0.20)	0.75 (0.10)	0.90 (0.20)	0.767 (0.26)

AUC, area under the curve; SD, Standard Deviation; SVC, Support Vector Classifier.

Table 4
Scores of the considered classifiers fitted with 4 wash-in and wash-out gland features, selected with MRMR. Mean and standard deviation (SD) values from the 10 cross validation splits of the dataset are reported.

Model	AUC	Accuracy	Sensitivity	Specificity
	Mean (SD)	Mean (SD)	Mean (SD)	Mean (SD)
SVC	0.78 (0.17)	0.73 (0.09)	0.85 (0.23)	0.82 (0.17)
Random Forest	0.73 (0.26)	0.73 (0.11)	0.85 (0.23)	0.79 (0.19)
Decision Tree	0.62 (0.20)	0.71 (0.13)	0.4 (0.37)	0.92 (0.10)
Logistic Regression	0.78 (0.17)	0.73 (0.13)	0.85 (0.23)	0.86 (0.16)

AUC, area under the curve; SD, Standard Deviation; SVC, Support Vector Classifier.

predicting the mutational status of BRCA1. In our study, among the 372 extracted radiomic features, eight features were sufficiently independent and carried most information to classify the BRCA mutational status allowing to avoid redundancy. The best features classifiers were SVC and Logistic Regression.

In the radiomics analysis both features extracted from the tumor and from the glandular tissue of the contralateral breast were considered, comparing BRCA1 mutated and non-mutated patients. In fact, among the eight informative features, four derived from the healthy gland and four from the tumor.

We observed that radiomic models fitted combining tumor and gland features or computed with gland features only obtained a satisfying performance (AUCs ranging from 0.78 to 0.80) in the discrimination between non BRCA-mutated and BRCA1-mutated patients. Radiomics analysis of normal glandular tissue and tumor in the dynamic contrast

MR-sequence was able to highlight significantly different elements between BRCA1 mutated and non-mutated patients. Instead, the model fitted with the features extracted from the tumor only was not able to discriminate between mutated and non-mutated patients.

Features both related to the contrastographic wash-in and wash-out map were analyzed and those significantly different in the two groups of women are all features related to the wash-out gland and tumor map.

Total energy and correlation, both extracted from wash out glandular tissue map, were significantly higher within BRCA1 mutated patients. Total Energy is a measure of the magnitude of voxel values, scaled by the volume of the voxel. BRCA1-mutated patients showed higher Total Energy in wash-out gland maps, suggesting that the contrast agent remained longer in glandular tissue of BRCA1-mutated than non-mutated patients. Therefore, we hypothesized that mutated patients may have a slower wash out of the gland. Also, Correlation from Gray Level Co-occurrence matrix was higher in BRCA1-mutated patients. Correlation shows the linear dependency of gray levels to their respective voxel in GLCM, hence the more the voxel intensity is correlated to its position, the greater the correlation will be. It follows that BRCA1-mutated patients showed a more regular pattern and a greater tissue homogeneity when releasing the contrast agent. This was true also for the wash-in maps, in which Correlation was higher for BRCA1-mutated patients, but the difference was not statistically significant. Overall, the radiomics texture of the glandular tissue enhancement in BRCA1 carriers showed values of greater intensity and higher homogeneity in the volume unit, which may possibly reflect a more regular microenvironment that retains the contrast medium for longer.

In agreement with our study, several works in literature have highlighted the relevance of these features in the construction of a radiomic signature that can fulfill both predictive and discriminative tasks in the oncology setting such as neurology, and gastroenterology [27–30].

The only feature from tumor segmentation selected by MRMR which differed significantly among BRCA1 mutated and non-mutated patients was Root Mean Squared, related to the magnitude of the wash-out map values, showing that also in the tumor district the BRCA1-mutated patients maintained a larger amount of contrast agent at the end of the scan. This feature appears in different works in predictive analyses of outcome and tumor aggressiveness falling within the lesion analysis of heterogeneity and entropy. For example, it emerged significant in predictive models linked to lung, cervical and stomach cancers [31–33].

This study has some limitations. Firstly, the retrospective nature of the study prevented us from adopting a standardized protocol in MRI examination. However, all the included studies were conducted on the same scanner and the use of DCE sequences with standardized acquisition parameters allowed us to minimize the effect of the retrospective design. Secondly, the sample size is limited and external validation is lacking.

5. Conclusions

In conclusion, in this study DCE-MRI radiomic models showed promising performance in the discrimination between non BRCA-mutated and BRCA1-mutated patients, especially for models fitted with features derived from both tumor and glandular tissue or from glandular tissue only. Differences in glandular radiomics features between mutated and non-mutated patients may reflect different tissue characteristics, likely involved in contrast media distribution, and possibly related to the genomic subgroup. The radiomic texture of the glandular tissue and of the tumor in the dynamic contrast sequence highlighted significant differences in women carrying the mutation compared to those without mutation, not detectable by the standard enhancement evaluation and tumors intensity-time curves.

Our study has highlighted the possibility to detect features related to the genomic assessment different between mutated and non-mutated patients in breast MR.

These results may contribute to the advancements in the field of breast radiogenomic but should be confirmed in larger and prospective studies with external validation cohorts.

Ethical statement

The study has been approved by the local ethical committee.

CRediT authorship contribution statement

Annarita Pecchi: Writing – original draft, Investigation, Data curation, Conceptualization. **Chiara Bozzola:** Writing – review & editing, Investigation, Data curation. **Cecilia Beretta:** Writing – review & editing, Investigation. **Giulia Besutti:** Writing – original draft, Methodology, Data curation, Conceptualization. **Angela Toss:** Writing – review & editing, Investigation, Conceptualization. **Laura Cortesi:** Writing – review & editing, Investigation, Conceptualization. **Erica Balboni:** Writing – review & editing, Software, Methodology, Investigation. **Luca Nocetti:** Writing – review & editing, Software, Methodology, Formal analysis. **Guido Ligabue:** Writing – review & editing, Investigation. **Pietro Torricelli:** Writing – review & editing, Supervision, Investigation.

Declaration of competing interest

The authors declare that they have no known competing financial interests or personal relationships that could have appeared to influence the work reported in this paper.

Acknowledgement

This study was partially supported by funding from the European Union-NextGenerationEU through the Italian Ministry of University and Research under PNRR -M4C2-I1.3 Project PE_00000019 “HEAL ITALIA” to Giulia Besutti, E93C22001860006.

Appendix A. Supplementary data

Supplementary data to this article can be found online at https://doi.org/10.1016/j.mri.2024.110214.

References

[1] Jiang L, You C, Xiao Y, et al. Radiogenomic analysis reveals tumor heterogeneity of triple-negative breast cancer. Cell Rep Med 2022;3:100694. https://doi.org/10.1016/j.xcrm.2022.100694.
[2] Yin L, Duan J-J, Bian X-W, Yu S-C. Triple-negative breast cancer molecular subtyping and treatment progress. Breast Cancer Res BCR 2020;22:61. https://doi.org/10.1186/s13058-020-01296-5.
[3] Petrucelli N, Daly MB, Pal T. BRCA1- and BRCA2-associated hereditary breast and ovarian cancer. In: Adam MP, Feldman J, Mirzaa GM, et al., editors. GeneReviews®. Seattle, Seattle (WA): University of Washington; 1993.
[4] Krainer M, Silva-Arrieta S, FitzGerald MG, et al. Differential contributions of BRCA1 and BRCA2 to early-onset breast cancer. N Engl J Med 1997;336:1416–21. https://doi.org/10.1056/NEJM199705153362003.
[5] Evans DG, Shenton A, Woodward E, et al. Penetrance estimates for BRCA1 and BRCA2 based on genetic testing in a clinical Cancer genetics service setting: risks of breast/ovarian cancer quoted should reflect the cancer burden in the family. BMC Cancer 2008;8:155. https://doi.org/10.1186/1471-2407-8-155.
[6] Atchley DP, Albarracin CT, Lopez A, et al. Clinical and pathologic characteristics of patients with BRCA-positive and BRCA-negative breast cancer. J Clin Oncol Off J Am Soc Clin Oncol 2008;26:4282–8. https://doi.org/10.1200/JCO.2008.16.6231.
[7] Lakhani SR, Van De Vijver MJ, Jacquemier J, et al. The pathology of familial breast cancer: predictive value of immunohistochemical markers estrogen receptor, progesterone receptor, HER-2, and p53 in patients with mutations in BRCA1 and BRCA2. J Clin Oncol Off J Am Soc Clin Oncol 2002;20:2310–8. https://doi.org/10.1200/JCO.2002.09.023.
[8] Incorvaia L, Fanale D, Bono M, et al. BRCA1/2 pathogenic variants in triple-negative versus luminal-like breast cancers: genotype-phenotype correlation in a cohort of 531 patients. Ther Adv Med Oncol 2020;12. https://doi.org/10.1177/1758835920975326. 1758835920975326.
[9] You C, Xiao Q, Zhu X, et al. The clinicopathological and MRI features of patients with BRCA1/2 mutations in familial breast cancer. Gland Surg 2021;10:262–72. https://doi.org/10.21037/gs-20-596.

[10] Noh JM, Han B-K, Choi DH, et al. Association between BRCA mutation status, pathological findings, and magnetic resonance imaging features in patients with breast cancer at risk for the mutation. J Breast Cancer 2013;16:308–14. https://doi.org/10.4048/jbc.2013.16.3.308.
[11] Cè M, Caloro E, Pellegrino ME, et al. Artificial intelligence in breast cancer imaging: risk stratification, lesion detection and classification, treatment planning and prognosis—a narrative review. Explor Target Anti-Tumor Ther 2022;3:795–816. https://doi.org/10.37349/etat.2022.00113.
[12] Gallivanone F, Bertoli G, Porro D. Radiogenomics, breast Cancer diagnosis and characterization: current status and future directions. Methods Protoc 2022;5:78. https://doi.org/10.3390/mps5050078.
[13] Mazurowski MA. Radiogenomics: what it is and why it is important. J Am Coll Radiol JACR 2015;12:862–6. https://doi.org/10.1016/j.jacr.2015.04.019.
[14] Satake H, Ishigaki S, Ito R, Naganawa S. Radiomics in breast MRI: current progress toward clinical application in the era of artificial intelligence. Radiol Med (Torino) 2022;127:39–56. https://doi.org/10.1007/s11547-021-01423-y.
[15] Tagliafico AS, Piana M, Schenone D, et al. Overview of radiomics in breast cancer diagnosis and prognostication. Breast Off J Eur Soc Mastology 2019;49:74–80. https://doi.org/10.1016/j.breast.2019.10.018.
[16] Bickelhaupt S, Paech D, Kickingereder P, et al. Prediction of malignancy by a radiomic signature from contrast agent-free diffusion MRI in suspicious breast lesions found on screening mammography. J Magn Reson Imaging JMRI 2017;46:604–16. https://doi.org/10.1002/jmri.25606.
[17] Petrillo A, Fusco R, Barretta ML, et al. Radiomics and artificial intelligence analysis by T2-weighted imaging and dynamic contrast-enhanced magnetic resonance imaging to predict breast cancer histological outcome. Radiol Med (Torino) 2023;128:1347–71. https://doi.org/10.1007/s11547-023-01718-2.
[18] Molinari C, Clauser P, Girometti R, et al. MR mammography using diffusion-weighted imaging in evaluating breast cancer: a correlation with proliferation index. Radiol Med (Torino) 2015;120:911–8. https://doi.org/10.1007/s11547-015-0527-z.
[19] Conti A, Duggento A, Indovina I, et al. Radiomics in breast cancer classification and prediction. Semin Cancer Biol 2021;72:238–50. https://doi.org/10.1016/j.semcancer.2020.04.002.
[20] Dong Y, Feng Q, Yang W, et al. Preoperative prediction of sentinel lymph node metastasis in breast cancer based on radiomics of T2-weighted fat-suppression and diffusion-weighted MRI. Eur Radiol 2018;28:582–91. https://doi.org/10.1007/s00330-017-5005-7.
[21] Kocak B, Baessler B, Bakas S, et al. CheckList for EvaluAtion of Radiomics research (CLEAR): a step-by-step reporting guideline for authors and reviewers endorsed by ESR and EuSoMII. Insights Imaging 2023;14:75. https://doi.org/10.1186/s13244-023-01415-8.
[22] Fedorov A, Beichel R, Kalpathy-Cramer J, et al. 3D slicer as an image computing platform for the quantitative imaging network. Magn Reson Imaging 2012;30:1323–41. https://doi.org/10.1016/j.mri.2012.05.001.
[23] Dietterich TG. Approximate statistical tests for comparing supervised classification learning algorithms. Neural Comput 1998;10(7):1895–923. https://doi.org/10.1162/089976698300017197.
[24] Veltman J, Mann R, Kok T, et al. Breast tumor characteristics of BRCA1 and BRCA2 gene mutation carriers on MRI. Eur Radiol 2008;18:931–8. https://doi.org/10.1007/s00330-008-0851-y.
[25] Kumar P, Aggarwal R. An overview of triple-negative breast cancer. Arch Gynecol Obstet 2016;293:247–69. https://doi.org/10.1007/s00404-015-3859-y.
[26] Whitman GJ, Albarracin CT, Gonzalez-Angulo AM. Triple-negative breast Cancer: what the radiologist needs to know. Semin Roentgenol 2011;46:26–39. https://doi.org/10.1053/j.ro.2010.09.004.
[27] Bobholz SA, Lowman AK, Barrington A, et al. Radiomic features of multiparametric MRI present stable associations with analogous histological features in patients with brain cancer. Tomography 2020;6:160–9. https://doi.org/10.18383/j.tom.2019.00029.
[28] Winkelmann MT, Gassenmaier S, Walter SS, et al. Differentiation of adrenal adenomas from adrenal metastases in single-phased staging dual-energy CT and radiomics. Diagn Interv Radiol Ank Turk 2022;28:208–16. https://doi.org/10.5152/dir.2022.21691.
[29] Yoon S, Kim YH, Lee Y, et al. Tumor heterogeneity in human epidermal growth factor receptor 2 (HER2)-positive advanced gastric cancer assessed by CT texture analysis: association with survival after Trastuzumab treatment. PLoS One 2016;11:e0161278. https://doi.org/10.1371/journal.pone.0161278.
[30] Pantic I, Pantic S, Paunovic J, Perovic M. Nuclear entropy, angular second moment, variance and texture correlation of thymus cortical and medullar lymphocytes: grey level co-occurrence matrix analysis. An Acad Bras Cienc 2013;85:1063–72. https://doi.org/10.1590/S0001-37652013005000045.
[31] Giganti F, Antunes S, Salerno A, et al. Gastric cancer: texture analysis from multidetector computed tomography as a potential preoperative prognostic biomarker. Eur Radiol 2017;27:1831–9. https://doi.org/10.1007/s00330-016-4540-y.
[32] Yusufaly TI, Zou J, Nelson TJ, et al. Improved prognosis of treatment failure in cervical cancer with nontumor PET/CT Radiomics. J Nucl Med Off Publ Soc Nucl Med 2022;63:1087–93. https://doi.org/10.2967/jnumed.121.262618.
[33] Pérez-Morales J, Tunali I, Stringfield O, et al. Peritumoral and intratumoral radiomic features predict survival outcomes among patients diagnosed in lung cancer screening. Sci Rep 2020;10:10528. https://doi.org/10.1038/s41598-020-67378-8.